
ChaosMining: A Benchmark to Evaluate Post-Hoc Local Attribution Methods in Low SNR Environments

Ge Shi, Ziwen Kan, Jason Smucny, Ian Davidson

Department of Computer Science

University of California, Davis

{geshi, zkan, jsmucny, indavidson}@ucdavis.edu

Abstract

In this study, we examine the efficacy of post-hoc local attribution methods in identifying features with predictive power from irrelevant ones in domains characterized by a low signal-to-noise ratio (SNR), a common scenario in real-world machine learning applications. We developed synthetic datasets encompassing symbolic functional, image, and audio data, incorporating a benchmark on the $(Model \times Attribution \times Noise Condition)$ triplet. By rigorously testing various classic models trained from scratch, we gained valuable insights into the performance of these attribution methods in multiple conditions. Based on these findings, we introduce a novel extension to the notable recursive feature elimination (RFE) algorithm, enhancing its applicability for neural networks. Our experiments highlight its strengths in prediction and feature selection, alongside limitations in scalability. Further details and additional minor findings are included in the appendix, with extensive discussions. The codes and resources are available at URL.

1 Introduction

The successful application of machine learning typically hinges on two complementary strategies: (I) identifying the most predictive features for learning referred to as the data-centric approach [51], and (II) training the model to approximate the optimal weights, known as the model-centric approach [30]. Both strategies are crucial for reducing generalization errors in predictive tasks, with feature engineering playing an essential role in this process [13].

Noisy or irrelevant features are prevalent in real-world applications [6]. Due to their robustness against noise, neural networks have become a common choice for analyzing low signal-to-noise ratio (SNR) data across various domains, including finance [37], clinical settings [15], and scientific research [10]. Whereas black-box models often suffice for multimedia data such as online images, videos, and text posts, low SNR domains demand high levels of explainability [35], underscoring the critical need for transparent methodologies. Nowadays, post-hoc local attribution is one of the most popular approaches in the eXplainable AI (XAI) taxonomy to achieve this goal [52, 53, 8, 23].

Post-hoc local attribution methods, which assign importance scores to individual features [2], are widely utilized to elucidate neural network preferences regarding input features. Despite their popularity, there appears to be a paucity of *rigorous quantitative* empirical research examining the ability of these methods to effectively differentiate between features with strong predictive capabilities and those that are irrelevant. This gap in the literature motivates our study.

In this research, we begin by conducting an empirical analysis to assess the effectiveness of using post-hoc attribution methods to differentiate between predictive and irrelevant features. Our study yields several noteworthy findings: (I) Gradient-based saliency alone is sufficient for feature selection, offering high precision, convergence, and low cost; (II) A significant positive correlation exists between the efficacy of post-hoc attribution methods and the generalization capabilities of the

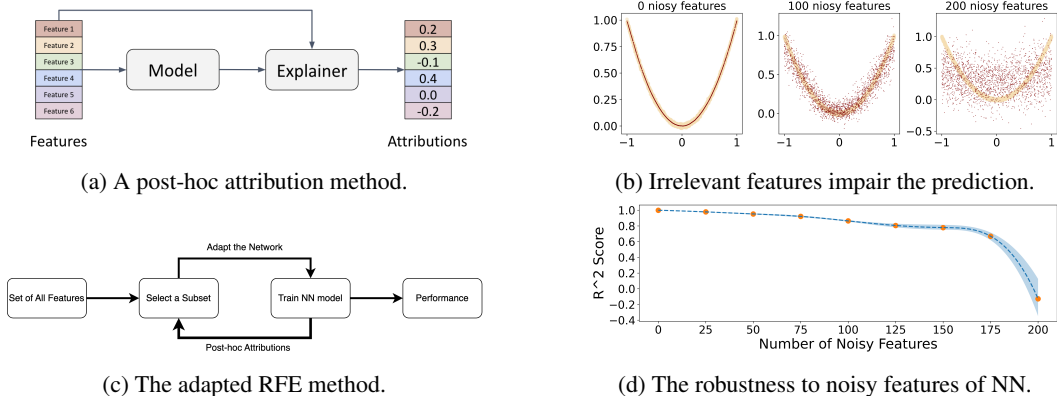


Figure 1: A teaser figure of the approach (on the left) and challenge (on the right) of this work. In (a) and (c), the attributions are scalar weights assigned to features via a one-to-one mapping in a post-hoc manner. In (b) and (d), only one feature is predictive as defined by Equation 1.

predictive model; (III) Neural networks are less susceptible to structural noise compared to random noise; (IV) Neural networks more effectively identify predictive features at fixed positions than those randomly distributed. Building on these insights, we further explore the inherent robustness of neural networks and the discriminative capacity of post-hoc attribution methods to enhance the recursive feature elimination (RFE) technique [9]. Our contributions are in three-folds:

- We created synthetic datasets for symbolic functional, image, and audio analysis, systematically blending predictive and irrelevant features. These datasets serve as accessible resources for researchers exploring this domain, facilitating downstream empirical studies.
- We evaluated the effectiveness of several well-known post-hoc attribution methods across various ($Model \times Attribution \times Noise Condition$) combinations within the curated datasets, uncovering several important but previously unnoticed insights.
- We adapted the Recursive Feature Elimination (RFE) strategy, traditionally applied to transparent models such as linear models, SVMs, and decision trees, for use with neural networks. Our empirical results highlight both the strengths and limitations of this approach.

2 Benchmark Procedure

The general procedure of the benchmark is data and ground truth annotation generation, metrics defining, model training, and post-hoc attribution methods evaluation. In this section, we focus on data generation and metrics defining.

2.1 Data Generation

We generate symbolic functional, vision, and audio data for downstream empirical studies to benchmark post-hoc attribution methods in various conditions. One novel and intriguing property of our synthetic dataset is the design of ($Model \times Attribution \times Noise Condition$) triplet. Beyond the ($Model \times Attribution$) paradigm adopted by other benchmarks, a noise condition factor is introduced. We design the data generation and empirical study to address the following questions: **Among the three factors, how does each of them affect the predictive feature identification ability of a post-hoc attribution method?**

To avoid misunderstanding about the triplet, we elucidate the concepts in this context separately.

- **Model.** A model embodies a trained checkpoint affected by the architecture (e.g. CNN-based, Transformer-based), the configuration (e.g. widths and depths of a model), and the hyper-parameters of training (e.g. learning rate, dropout rate).
- **Attribution.** Among the various feature attribution methods, we specifically study Saliency (SA), DeepLift (DL), Integrated Gradient (IG), and Feature Ablation (FA), which are model-agnostic

to all NN-based models for fair comparison across models. SA is the pure gradient. DL is a backpropagation-based approach. IG is a gradient-based approach referring to baseline data. FA is a perturbation-based approach. As for detailed definitions, please refer to the appendix.

- **Noise condition.** Noise conditions include but are not limited to the type of noise, the signal-to-noise ratio, the magnitude of label noise, and the way that features are aligned across instances.

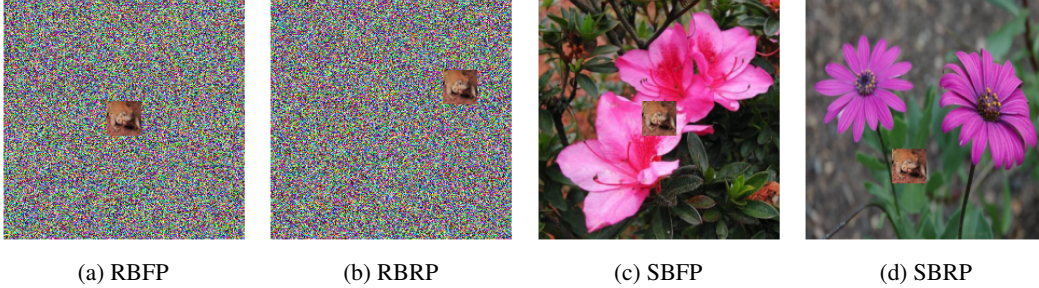


Figure 2: The examples of synthetic vision data and saliency maps of attribution methods. The foreground images can be placed at a fixed position (center) across instances or randomly. The background images can be generated by Gaussian noise or images of flowers.

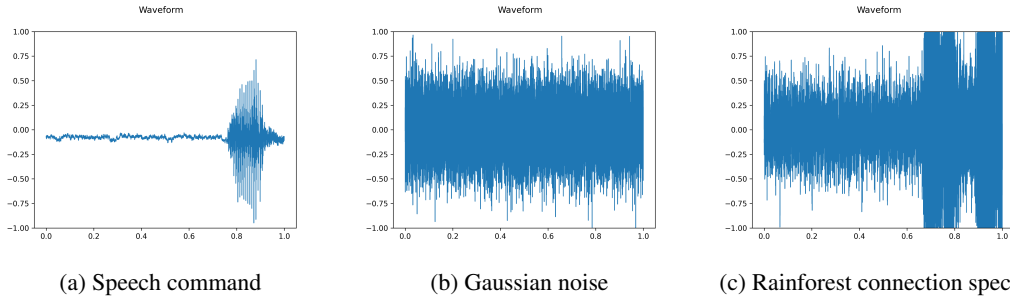


Figure 3: The examples of sources to construct synthetic audio data. Figure (a) is the foreground predictive feature while (b) and (c) are background features that are irrelevant to the classification task.

To conduct more synthesized experiments on multiple modalities and raise broader interest, we enrich the context by generating three different types of synthetic data. Specifically, we created

Symbolic functional data (e.g. Equation 1) based on human-designed symbolic functions with ground truth annotations derived from math formulas. It’s used to study the general behaviors of multilayer perceptron (MLP) networks on regression tasks. Each input sample is a vector of length n with m of them determining the target value for prediction. To generate a sample from a function with m predictive features, the value of each feature is drawn from a normal distribution $\mathcal{N}(\mu, \sigma^2)$, where $\mu = 0, \sigma = 1$. The regression target y is numerically computed from the first m features. A naive example can be an intrinsic single variate symbolic quadratic function with m noisy features.

$$y = x_0^2, x = [x_0, x_1, \dots, x_m] \quad (1)$$

Vision data (e.g. Figure 2) is used to study popular architectures for visual scene classification tasks. Each noisy input sample is in the form of a 224×224 image. A noisy image is generated by replacing a portion of a background image with a 32×32 foreground image. The prediction task is to predict the label of the foreground image. The foreground images are randomly sampled from the **CIFAR-10** [20] dataset. There are two types of background images, (I) a random noisy image generated from the same normal distribution as in the symbolic functional data generation (**RB**); (II) a structural noisy image randomly drawn from the **Flower102** [29] dataset (**SB**). The position of where the foreground image is placed is documented. Based on whether they are placed in the same position across all instances, there are two conditions, (I) the positions of all foreground images are fixed in the center of the background images (**FP**); (II) the positions of all foreground images are randomly scattered (**RP**).

Table 1: The design of the triplets. All four attribution methods (SA, DL, IG, FA) are used for every condition, so we don’t include them in the table for simplicity.

Data	Models	Noise Conditions
Symbolic	configurations, hyper-parameters	feature noise, label noise
Vision	CNNs, ViTs	random/structure noise, random/fixed position
Audio	RNNs, Transformer	random/structure noise

Audio data (e.g. Figure 3) is used to study popular architectures for sequential data classification tasks. Each noisy input sample is a 10-channel waveform audio sequence with a 16,000 sampling rate. Similar to the vision data, each sequence consists of a foreground audio and a background audio splitter by channels. In each sample, only the first channel carries the foreground audio drawn from the **Speech Command** [48] dataset which indicates the prediction task. All the other channels are considered as noises. Based on how the background noise is created, the noise conditions can be divided into (I) random audio generated from a normal distribution (**RB**); (II) the audio randomly drawn from the **Rainforest Connection Species** [49] dataset (**SB**). We also studied the fixed position vs. random position conditions for the audio data. However, since all the models failed to learn meaningful predictions, we dropped these conditions with little significance.

2.2 Metrics

In addition to traditional metrics like accuracy and mean absolute error (MAE), we introduce two additional metrics for a more comprehensive evaluation.

Uniform Score (UScore) is a modified version of the Mean Absolute Error (MAE) that normalizes it into the range (0, 1). We employ this metric to assess the proximity of predictions to the true symbolic values. We prefer the UScore over MAE in our multiple regression tasks, as detailed in 2.1, because using MAE could result in excessively varied scales across different tasks. To ensure a fair summary and consistent comparison, we propose the Uniform Score, which is defined as follows:

$$UScore = \frac{1}{N} \sum_{i=1}^N \left(1 - \frac{|\hat{y}_i - y_i|}{|\hat{y}_i| + |y_i| + \epsilon}\right), \quad (2)$$

where \hat{y}_i represents the predicted value and y_i denotes the ground truth target value for the i -th instance in a dataset consisting of N samples.

Functional Precision (FPrec) quantifies the overlap between the k predictive features given by annotation and those deemed top- k important by a model, as ranked by the post-hoc attribution method. This approach is akin to the feature agreement measure introduced by [19], effectively integrating both precision and recall aspects into a single metric.

$$FPrec = \frac{|\{\text{top-}k \text{ features of model}\} \cap \{k \text{ predictive features}\}|}{k} \quad (3)$$

We will talk about other metrics in Section 3 along with experimental results.

3 Experiments and insights

Building on the benchmark pipeline outlined in the previous section, we conducted a series of evaluation experiments. In this section, we discuss experimental results and observations¹, addressing several pertinent research questions and providing insights that may inform future studies. We present the experiment of each modality separately. Experiments are repeated 5 times with random seeds.

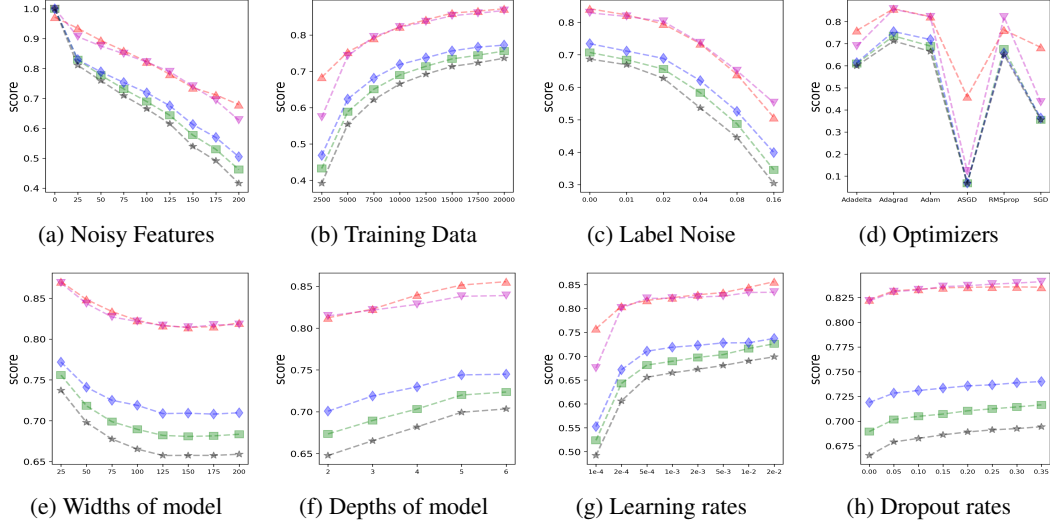


Figure 4: Experimental results on symbolic functional data using MLP regressors differentiated by varying factors. For each subplot, we only change one factor from the default configuration. \blacktriangle denotes the $UScore$ of the predictions. \blacktriangledown , \blacksquare , \blacklozenge , and \blackstar denote the $FPrec$ of SA, DL, IG, and FA methods respectively.

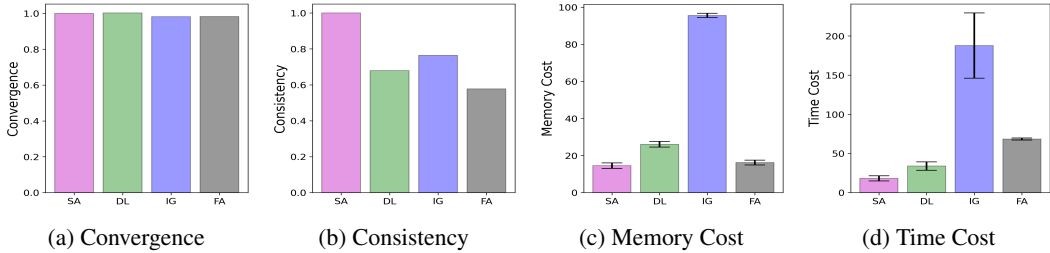


Figure 5: The results of our simulation experiments. Convergence is quantified by the area under the $FPrec$ curve across 300 training epochs, while consistency is assessed through the average agreement between the top-k most important features of a sample and the average importance of the entire dataset. Both convergence and consistency scores are normalized so that the value for SA is set to 1. Additionally, we report the average and standard deviation of the memory and time costs incurred at the test stage.

3.1 Symbolic Functional Data Experiment

We conducted a series of experiments to assess the performance of neural network models and attribution methods under various configurations. Each experiment altered only one aspect of our standard setup, allowing us to isolate the impact of individual factors. Our default configuration included a dataset size of 10,000, a 4:1 train-test split, 100 noisy features, label noise set at 0.01, model dimensions with widths of 100 and depths of 3, an Adam optimizer, a learning rate of 0.001, no dropout, and a training duration of 1000 epochs targeting mean squared error loss. We reported the $UScore$ of the model and $FPrec$ of the attribution methods.

From the analysis of plots in Figure 4, we observe consistent trends across most figures, with a few exceptions like FA in Figure 4h. Two key insights emerge. (I) **SA consistently outperforms other attribution methods in low SNR environments, as measured by $FPrec$.** (II) **The effectiveness of all XAI methods is closely tied to the model’s predictive capabilities.** Additionally, enhancements in regression model performance were noted with reductions in noisy features and label noise and increases in dataset size, model depth, learning rate, and dropout rate. However, wider models (models with larger widths), despite having greater capacity, showed diminished predictive accuracy, possibly due to more neurons in a layer learning to memorize noise features and their nuanced internal correlation rather than the real underlying patterns. In tests with default Pytorch optimizers, as shown

¹We did not investigate transformer-based large models due to their limited adoption in Low SNR domains like finance, science, and clinical areas except for natural language processing.

Table 2: Experimental results (Top-1 classification accuracy and attribution IoU) on synthetic vision data with random background noise.

Architecture	GFLOPs	RBFP					RBRP				
		Pred(ACC%)	SA(IoU)	DL(IoU)	IG(IoU)	FA(IoU)	Pred(ACC%)	SA(IoU)	DL(IoU)	IG(IoU)	FA(IoU)
AlexNet [21]	0.71	10.00±0.000	0.021±0.000	0.011±0.101	0.012±0.086	0.021±0.000	10.00±0.000	0.021±0.000	0.018±0.002	0.023±0.002	0.021±0.000
DenseNet121 [16]	2.83	83.38±0.175	0.738±0.027	0.566±0.090	0.601±0.036	0.748±0.003	82.07±0.429	0.699±0.003	0.367±0.091	0.372±0.119	0.362±0.001
GoogleNet [44]	1.5	79.03±0.129	0.703±0.012	0.287±0.176	0.302±0.207	0.699±0.018	77.88±0.484	0.699±0.008	0.275±0.0076	0.279±0.186	0.369±0.006
ResNet18 [12]	1.81	77.44±0.164	0.678±0.017	0.530±0.033	0.551±0.023	0.677±0.022	76.26±0.223	0.659±0.008	0.393±0.105	0.287±0.029	0.321±0.005
ResNet50 [12]	4.09	83.23±0.015	0.656±0.034	0.326±0.014	0.457±0.153	0.682±0.043	82.06±0.390	0.681±0.007	0.289±0.078	0.207±0.065	0.334±0.003
Vgg13 [40]	11.31	10.00±0.000	0.021±0.000	0.011±0.009	0.021±0.000	0.010±0.005	10.00±0.000	0.021±0.000	0.015±0.005	0.006±0.000	0.016±0.003
Vit_b_16 [11]	17.56	48.05±1.544	0.085±0.008	0.148±0.034	0.117±0.016	0.369±0.038	24.53±0.039	0.049±0.004	0.071±0.008	0.065±0.006	0.054±0.010
Vit_l_32 [11]	61.55	53.27±1.376	0.201±0.036	0.273±0.093	0.269±0.028	0.709±0.088	17.10±0.111	0.043±0.006	0.072±0.010	0.071±0.010	0.061±0.013

Table 3: Experimental results (Top-1 classification accuracy and attribution IoU) on vision data with structural background noise.

Architecture	GFLOPs	SBFP					SBRP				
		Pred(ACC%)	SA(IoU)	DL(IoU)	IG(IoU)	FA(IoU)	Pred(ACC%)	SA(IoU)	DL(IoU)	IG(IoU)	FA(IoU)
AlexNet [21]	0.71	10.00±0.000	0.021±0.000	0.021±0.000	0.017±0.055	0.021±0.000	10.00±0.000	0.021±0.000	0.021±0.000	0.021±0.000	0.021±0.000
DenseNet121 [16]	2.83	85.60±0.240	0.767±0.002	0.645±0.008	0.658±0.019	0.857±0.003	84.23±0.174	0.681±0.024	0.599±0.013	0.608±0.040	0.400±0.013
GoogleNet [44]	1.5	81.19±0.397	0.780±0.003	0.570±0.035	0.572±0.032	0.819±0.004	79.42±0.355	0.731±0.005	0.519±0.041	0.515±0.043	0.402±0.003
ResNet18 [12]	1.81	80.41±0.175	0.745±0.002	0.610±0.023	0.618±0.018	0.825±0.006	77.56±0.392	0.637±0.011	0.509±0.026	0.514±0.045	0.381±0.008
ResNet50 [12]	4.09	87.71±0.055	0.762±0.002	0.643±0.019	0.680±0.034	0.863±0.011	85.09±0.086	0.675±0.011	0.565±0.038	0.613±0.023	0.417±0.001
Vgg13 [40]	11.31	10.00±0.000	0.021±0.000	0.019±0.001	0.014±0.062	0.016±0.005	10.00±0.000	0.021±0.000	0.015±0.006	0.016±0.005	0.015±0.004
Vit_b_16 [11]	17.56	52.50±1.420	0.671±0.012	0.364±0.056	0.485±0.064	0.752±0.005	22.59±0.609	0.178±0.006	0.090±0.026	0.085±0.011	0.097±0.010
Vit_l_32 [11]	61.55	53.78±0.695	0.723±0.061	0.273±0.056	0.375±0.023	0.542±0.104	13.92±1.754	0.101±0.031	0.058±0.015	0.054±0.020	0.057±0.015

in Figure 4d, ASGD was notably ineffective at learning weights potentially due to the oscillation of gradients.

Additionally, we aim to determine which attribution methods converge more rapidly across epochs, maintain greater consistency across samples, and utilize fewer computational resources. As depicted in Figure 5, all four methods exhibit similar convergence rates, corresponding to the model training progression. **SA demonstrates significantly better consistency compared to the other three methods.** In terms of computational efficiency, IG consumes considerably more memory and time, while SA proves to be the most resource-efficient. Thus, we concluded that the naive SA method is the best considering all the factors.

3.2 Vision Data Experiment

For the vision task, we evaluated eight different architectures under four noise conditions, as detailed in Tables 2 and 3. All models underwent 30 epochs of training using the AdamW optimizer and a cosine annealing with warm restarts scheduler, with learning rates set to 0.001. The models were tested to identify the top-k important features, where k corresponds to the number of foreground image pixels forming a rectangle. Using these features, we determined the minimum bounding rectangle and calculated the intersection over union (IOU) score with the ground truth to assess the performance of attribution methods. Notably, AlexNet and Vgg13 failed to converge in all experiments, merely producing random guesses, likely due to the absence of skip connections. We observed that only SA consistently reported an even distribution of attributions, indicating no intrinsic inductive bias, unlike other methods. Moreover, SA generally outperformed other attribution methods, aligning with results from the symbolic functional data experiments.

Impact of structural vs. random background noise : Surprisingly, **neural networks (NNs) generally perform better at filtering out structural noise compared to random noise.** Similarly, all attribution methods demonstrated enhanced performance with structural noise. However, the performance improvement varied significantly among different attribution methods. SA showed only modest gains, whereas other methods improved substantially. Notably, the FA method outperformed SA on structural backgrounds (SBFP), possibly because patch-ablation-based FA, which interprets patches of pixels rather than individual pixels, is more effective at handling structural noises due to their semantic coherence.

Impact of predictive features at random vs. fixed positions : Both neural networks and attribution methods show improved performance for predictive features at fixed positions, a trend that is particularly pronounced in Vision Transformers (ViTs). This could be due to two main factors: First, position encoding in ViTs may be less effective at integrating positional information into the input. Second, the pixel patches ViTs analyze often include a mix of irrelevant and predictive features. This effect is also observed in attribution methods, where performance in the SBFP condition is

Table 4: Experimental results (classification Top-1 accuracy and FPrec) on synthetic audio data with the foreground signal at a fixed position.

Architecture	GFLOPs	RBFP					SBFP				
		Pred(ACC%)	SA(FPrec)	DL(FPrec)	IG(FPrec)	FA(FPrec)	Pred(ACC%)	SA(FPrec)	DL(FPrec)	IG(FPrec)	FA(FPrec)
RNN [26]	6.86	67.00 \pm 0.135	0.653 \pm 0.129	0.585 \pm 0.091	0.275 \pm 0.170	0.447 \pm 0.009	63.16 \pm 0.105	0.644 \pm 0.113	0.541 \pm 0.044	0.340 \pm 0.092	0.482 \pm 0.005
LSTM [36]	9.00	73.77 \pm 2.605	0.684 \pm 0.014	0.590 \pm 0.019	0.260 \pm 0.006	0.515 \pm 0.010	76.07 \pm 0.190	0.810 \pm 0.012	0.772 \pm 0.001	0.439 \pm 0.002	0.546 \pm 0.009
TCN [17]	6.73	80.96 \pm 1.237	0.641 \pm 0.005	0.297 \pm 0.006	0.258 \pm 0.002	0.539 \pm 0.003	82.52 \pm 0.185	0.721 \pm 0.007	0.427 \pm 0.009	0.337 \pm 0.005	0.561 \pm 0.023
Transformer [46]	29.7	23.25 \pm 0.756	0.460 \pm 0.010	0.236 \pm 0.015	0.138 \pm 0.004	0.335 \pm 0.008	25.75 \pm 0.320	0.513 \pm 0.054	0.315 \pm 0.007	0.193 \pm 0.006	0.373 \pm 0.007

significantly better than in others. Specifically, ViT_l_32 outperforms ViT_b_16 in fixed position scenarios but is less effective with random positions, likely because smaller patches include fewer patch-level noises when the foreground moves. Interestingly, even though CNN-based models are theoretically invariant to translation, they too perform better in fixed position conditions, aligning with findings from [5].

In summary, two broad observations emerge from our analysis: (I) **Among various attribution methods, SA almost always outperforms the other three methods.** (II) **Neural networks demonstrate superior performance when irrelevant features are structural and positioned fixedly.**

3.3 Audio Data Experiment

Similar to our vision data experiments, we also explored the effects of random versus structural noise on multi-channel time-series data, training each model with the AdamW optimizer and cosine annealing with warm restarts scheduler. The learning rate for the transformer is 0.0001 while the others are 0.001. The results are detailed in Table 4. We applied attribution methods to this data, aggregating absolute attributions across each channel, with channel importance calculated by $\sum_{t=1}^T |a_{\hat{c},t}| / \sum_{c=1}^C \sum_{t=1}^T |a_{c,t}|$.

Temporal convolutional neural networks (TCN) significantly outperformed other models, likely due to their convolution’s transition-invariant properties, which effectively encode learning biases. Similar to our findings in vision data, models and attribution methods showed better performance with structural noise compared to random noise. This could be because structural data is more easily encoded and recognized by the networks. Integrated gradients underperformed relative to other methods across all models, potentially due to two factors: (I) The use of a zero baseline might introduce bias, and (II) integrating gradients along a straight pathway could deviate from the data manifold, leading to errors.

4 Feature Selection with Neural Networks and Post-hoc Attributions

Feature selection, as surveyed by [27], aims to reduce the number of input variables for building predictive models. Traditional machine learning methods commonly employ techniques such as univariate filtering, embedding, and wrapper methods. A key wrapper method is Recursive Feature Elimination (RFE), which starts with all features and iteratively removes the least important ones based on model coefficients that signify feature importance. However, RFE’s reliance on model transparency limits its direct application to neural networks, which are typically opaque. To bridge this gap, we introduce an adaptation known as Recursive Feature Elimination with Neural Networks and Post-hoc Attribution (**RFEwNA**), detailed in Algorithm 1, enabling RFE’s application in more complex, black-box models.

In this section, we extend our analysis by integrating neural networks with attribution methods into the feature selection pipeline, transforming it from an open-loop system (see Figure 1a) to a closed-loop system (see Figure 1c). We conduct experiments using all four attribution methods across both classification and regression tasks. We compare our approach against traditional Recursive Feature Elimination (RFE) methods using statistical models such as linear models, decision trees (DT), and support vector machines (SVM). We anticipate that this closed-loop configuration will yield better prediction accuracy and more effectively identify relevant features.

4.1 RFEwNA on Classification

We solved a binary classification task to predict customer satisfaction utilizing the Santander Customer Satisfaction dataset [42]. The dataset comprises 369 features, which underwent min-max scaling preprocessing. Due to the dataset’s highly imbalanced labels and the unavailability of original test

Algorithm 1 RFEwNA

Input: Dataset X with m features, an neural networks model F , an post-hoc attribution explainer g

Parameter: Drop feature rate $dr\%$, target number of features k

Output: Dataset X^* with selected features, trained model F^*

- 1: Start with the full set of m features
 - 2: **while** Number of features in the selected set is greater than k **do**
 - 3: Train and evaluate F on X
 - 4: Evaluate the importance of each feature on the validation set with g
 - 5: Remove the least important $dr\%$ features from the selected set
 - 6: **end while**
-

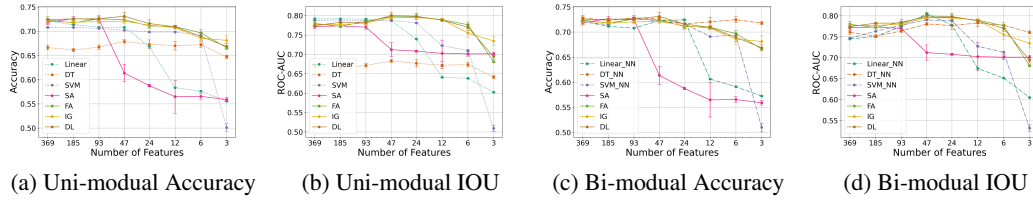


Figure 6: The performance of RFE on Santander Customer Satisfaction dataset. Figure 6a and Figure 6b show the test performance of using the same classifier (dotted line) for both RFE and final classification. As a comparison, Figure 6c and Figure 6d show the test performance of using a classifier (dash-dot line) for RFE and train a neural network for the final classification.

labels, we performed random undersampling on the training data of the majority class, resulting in 6,016 instances. Then it is split into 80% training data and 20% validation data.

To assess the effectiveness of RFEwNA, we conducted experiments using a drop rate $dr = 50\%$ and targeting three features ($k=3$). We repeated each experiment 5 times with randomness. We report validation accuracy and intersection over union metrics. In these tests, the same classifier was used for both feature selection and making predictions, a method we refer to as the uni-module strategy. Our interest lies in both the peak performance as the number of features decreases and the outcomes when only a few predictive features remain. As indicated in Figures 6a and 6b, the FA, IG, and DL methods consistently outperform traditional statistical models, **indicating our method is better in prediction than classic RFE**. One might question whether this superiority stems merely from the inherent predictive strength of neural networks over statistical models. To validate the efficacy of our feature selection, we implemented a bi-module strategy: selecting features using statistical models and then training a neural network on these features. This approach was then compared against the uni-module strategy. Results shown in Figures 6c and 6d demonstrate that RFEwNA significantly surpasses the performance of linear and SVM models. Notably, the decision tree model not only achieves comparable outcomes but also excels when the feature count is drastically reduced. **It means the selected features of our method are also more predictive than the original RFE.**

4.2 RFEwNA on Regression

We conducted empirical tests of our algorithm on the last five functions from our symbolic functional data, as referenced in 2.1, comparing it to the methodologies applied in the classification task. We assessed three key metrics: predictive performance measured by mean absolute error (MAE), feature selection efficacy via functional precision (FPrec), and computational cost using running time. Our method not only reduces MAE significantly (see Figure 7a), indicating superior accuracy but also outperforms RFE in feature selection across all tests (see Figure 7b). However, Figure 7c shows that despite GPU acceleration, our methods are more time-intensive.

In summary, **RFEwNA outperforms RFE in both prediction accuracy and feature selection, but at a significantly higher computational cost.** It is most suitable for small-scale datasets or scenarios where enhanced performance justifies the extra resource expenditure.

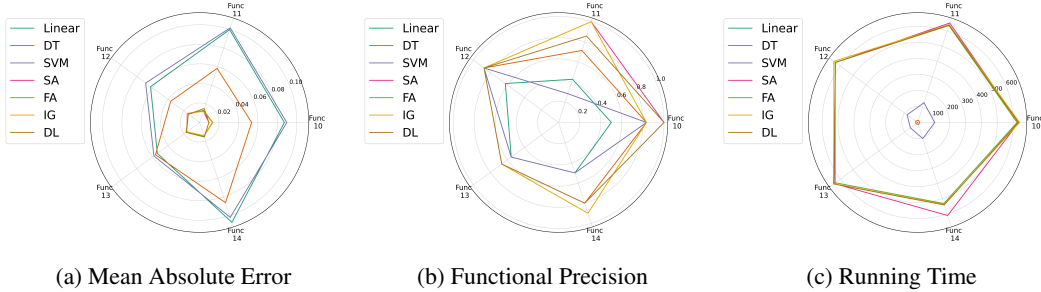


Figure 7: The performance of RFE on the last 5 synthetic symbolic functional data. Figure 7a shows the test *MAE* as the result of feature selection and regressor training. The smaller the value, the better the performance. Figure 7b shows the test *FPrec* as the result of feature selection. The larger the value, the better the performance. Figure 7c shows the logarithmic transformed test *running time* (s) which is $\log(1 + T)$.

5 Related Works

Existing research has established benchmarks for various XAI methods. Our work uniquely assesses predictive feature selection in post-hoc attribution methods across different modalities and models in low SNR environments. In contrast, [28, 38, 7] focus on other types of explanations like counterfactual or global explanations; [24, 1, 45] target specific domains such as medical or tabular data; [33, 47, 18] explore different model types such as graph neural networks or visual language models; [14, 22, 4] examine other aspects of attribution methods like faithfulness and fairness. Besides, we are the first to integrate the attributions in the recursive feature elimination pipeline.

6 Discussion and Conclusion

Ethical statement. Our dataset and study don't contain any harmful or restricted content. The code, data, and instructions to reproduce the main experimental results are at URL under a CC BY-NC 4.0 license. Due to the space limitation, we present more details about the dataset, models, training, and computing resources in the appendix. This research utilized and curated several open public datasets including the "Oxford 102 Flower" [29], "CIFAR-10" [20], "Speech Commands" [48], and the "Rainforest Connection Species Audio" [49] for which we gratefully acknowledge the respective contributors and maintainers for making these valuable resources available to the academic community.

Limitations and future work. The research presented here identifies several areas for further exploration and improvement. Firstly, while our analysis covered four distinct attribution methods, there remains a wealth of other significant techniques, such as SHAP [25], CAM [54], LIME [34], MAPLE [32], and LRP [3], that warrant investigation in future studies. Secondly, our explorations were limited to specific models, hyperparameters, and noise levels in vision and audio data. This constraint underscores the necessity to expand our dataset and experimental framework to include a wider variety of configurations. Thirdly, in the datasets we used, predictive accuracy was generally tied to isolated regions or channels rather than combinations of multiple predictive features. To enhance the generalizability and impact of the XAI benchmark, future work will aim to incorporate a more diverse array of attributions, models, and noise conditions.

Conclusion. Our paper explores the performance of neural network models and attribution methods under various configurations, providing key insights into their operational effectiveness. We have discovered that saliency attribution (SA) excels in low signal-to-noise ratio (SNR) environments and that the predictive capabilities of models significantly influence the effectiveness of XAI methods. Our research also underscores the differential impact of structural versus random background noise, with neural networks demonstrating enhanced proficiency in filtering out structural noise. Additionally, we explore leveraging attribution methods to adapt the RFE approach, seeing that the adapted method is better in prediction and feature selection yet computation-costly. Our study may have a broad impact on both algorithm design and feature selection on machine learning applications in financial, clinical, and scientific domains.

References

- [1] Chirag Agarwal, Dan Ley, Satyapriya Krishna, Eshika Saxena, Martin Pawelczyk, Nari Johnson, Isha Puri, Marinka Zitnik, and Himabindu Lakkaraju. Openxai: Towards a transparent evaluation of model explanations, 2024.
- [2] Marco Ancona, Enea Ceolini, Cengiz Öztireli, and Markus Gross. Towards better understanding of gradient-based attribution methods for deep neural networks. *arXiv preprint arXiv:1711.06104*, 2017.
- [3] Sebastian Bach, Alexander Binder, Grégoire Montavon, Frederick Klauschen, Klaus-Robert Müller, and Wojciech Samek. On pixel-wise explanations for non-linear classifier decisions by layer-wise relevance propagation. *PLoS one*, 10(7):e0130140, 2015.
- [4] Mohamed Karim Belaid, Richard Bornemann, Maximilian Rabus, Ralf Krestel, and Eyke Hüllermeier. Compare-xai: Toward unifying functional testing methods for post-hoc xai algorithms into a multi-dimensional benchmark. In *World Conference on Explainable Artificial Intelligence*, pages 88–109. Springer, 2023.
- [5] Valerio Biscione and Jeffrey S. Bowers. Convolutional neural networks are not invariant to translation, but they can learn to be, 2021.
- [6] Cesar F Caiafa, Zhe Sun, Toshihisa Tanaka, Pere Martí-Puig, and Jordi Solé-Casals. Machine learning methods with noisy, incomplete or small datasets, 2021.
- [7] Stephen Casper, Yuxiao Li, Jiawei Li, Tong Bu, Kevin Zhang, and Dylan Hadfield-Menell. Benchmarking interpretability tools for deep neural networks. *arXiv e-prints*, pages arXiv–2302, 2023.
- [8] Jिंगgang Chen, Junjie Li, Xiaoyang Qu, Jianzong Wang, Jiguang Wan, and Jing Xiao. Gaia: Delving into gradient-based attribution abnormality for out-of-distribution detection, 2024.
- [9] Xue-wen Chen and Jong Cheol Jeong. Enhanced recursive feature elimination. In *Sixth International Conference on Machine Learning and Applications (ICMLA 2007)*, pages 429–435, 2007. doi: 10.1109/ICMLA.2007.35.
- [10] Yangkang Chen, Mi Zhang, Min Bai, and Wei Chen. Improving the signal-to-noise ratio of seismological datasets by unsupervised machine learning. *Seismological Research Letters*, 90(4):1552–1564, 2019.
- [11] Alexey Dosovitskiy, Lucas Beyer, Alexander Kolesnikov, Dirk Weissenborn, Xiaohua Zhai, Thomas Unterthiner, Mostafa Dehghani, Matthias Minderer, Georg Heigold, Sylvain Gelly, et al. An image is worth 16x16 words: Transformers for image recognition at scale. *arXiv preprint arXiv:2010.11929*, 2020.
- [12] Kaiming He, Xiangyu Zhang, Shaoqing Ren, and Jian Sun. Deep residual learning for image recognition. In *Proceedings of the IEEE conference on computer vision and pattern recognition*, pages 770–778, 2016.
- [13] Jeff Heaton. An empirical analysis of feature engineering for predictive modeling. In *SoutheastCon 2016*, pages 1–6. IEEE, 2016.
- [14] Anna Hedström, Leander Weber, Daniel Krakowczyk, Dilyara Bareeva, Franz Motzkus, Wojciech Samek, Sebastian Lapuschkin, and Marina M.-C. Hähnle. Quantus: An explainable ai toolkit for responsible evaluation of neural network explanations and beyond. *Journal of Machine Learning Research*, 24(34): 1–11, 2023. URL <http://jmlr.org/papers/v24/22-0142.html>.
- [15] Roberto Holgado-Cuadrado, Carmen Plaza-Seco, Lisandro Lovisolo, and Manuel Blanco-Velasco. Characterization of noise in long-term ecg monitoring with machine learning based on clinical criteria. *Medical & Biological Engineering & Computing*, 61(9):2227–2240, 2023.
- [16] Gao Huang, Zhuang Liu, Laurens Van Der Maaten, and Kilian Q Weinberger. Densely connected convolutional networks. In *Proceedings of the IEEE conference on computer vision and pattern recognition*, pages 4700–4708, 2017.
- [17] Nal Kalchbrenner, Lasse Espeholt, Karen Simonyan, Aaron van den Oord, Alex Graves, and Koray Kavukcuoglu. Neural machine translation in linear time. *arXiv preprint arXiv:1610.10099*, 2016.
- [18] Sunnie SY Kim, Nicole Meister, Vikram V Ramaswamy, Ruth Fong, and Olga Russakovsky. Hive: Evaluating the human interpretability of visual explanations. In *European Conference on Computer Vision*, pages 280–298. Springer, 2022.
- [19] Satyapriya Krishna, Tessa Han, Alex Gu, Javin Pombra, Shahin Jabbari, Steven Wu, and Himabindu Lakkaraju. The disagreement problem in explainable machine learning: A practitioner’s perspective. *arXiv preprint arXiv:2202.01602*, 2022.

- [20] Alex Krizhevsky. Learning multiple layers of features from tiny images. pages 32–33, 2009. URL <https://www.cs.toronto.edu/~kriz/learning-features-2009-TR.pdf>.
- [21] Alex Krizhevsky, Ilya Sutskever, and Geoffrey E Hinton. Imagenet classification with deep convolutional neural networks. *Advances in neural information processing systems*, 25, 2012.
- [22] Xuhong Li, Mengnan Du, Jiamin Chen, Yekun Chai, Himabindu Lakkaraju, and Haoyi Xiong. M4: A unified xai benchmark for faithfulness evaluation of feature attribution methods across metrics, modalities and models. *Advances in Neural Information Processing Systems*, 36, 2023.
- [23] Shuyang Liu, Zixuan Chen, Ge Shi, Ji Wang, Changjie Fan, Yu Xiong, Runze Wu Yujing Hu, Ze Ji, and Yang Gao. A new baseline assumption of integrated gradients based on shaply value, 2024.
- [24] Yang Liu, Sujay Khandagale, Colin White, and Willie Neiswanger. Synthetic benchmarks for scientific research in explainable machine learning. *arXiv preprint arXiv:2106.12543*, 2021.
- [25] Scott M Lundberg and Su-In Lee. A unified approach to interpreting model predictions. *Advances in neural information processing systems*, 30, 2017.
- [26] Larry R Medsker and LC Jain. Recurrent neural networks. *Design and Applications*, 5(64-67):2, 2001.
- [27] Jianyu Miao and Lingfeng Niu. A survey on feature selection. *Procedia computer science*, 91:919–926, 2016.
- [28] Catarina Moreira, Yu-Liang Chou, Chihcheng Hsieh, Chun Ouyang, Joaquim Jorge, and João Madeiras Pereira. Benchmarking counterfactual algorithms for xai: From white box to black box, 2022.
- [29] Maria-Elena Nilsback and Andrew Zisserman. Automated flower classification over a large number of classes. In *Indian Conference on Computer Vision, Graphics and Image Processing*, Dec 2008.
- [30] Chanjun Park, Minsoo Khang, and Dahyun Kim. Model-based data-centric ai: Bridging the divide between academic ideals and industrial pragmatism, 2024.
- [31] Joelle Pineau, Philippe Vincent-Lamarre, Koustuv Sinha, Vincent Larivière, Alina Beygelzimer, Florence d’Alché Buc, Emily Fox, and Hugo Larochelle. Improving reproducibility in machine learning research (a report from the neurips 2019 reproducibility program). *Journal of Machine Learning Research*, 22(164): 1–20, 2021.
- [32] Gregory Plumb, Denali Molitor, and Ameet Talwalkar. Model agnostic supervised local explanations, 2019.
- [33] Mandeep Rathee, Thorben Funke, Avishek Anand, and Megha Khosla. Bagel: A benchmark for assessing graph neural network explanations. *arXiv preprint arXiv:2206.13983*, 2022.
- [34] Marco Tulio Ribeiro, Sameer Singh, and Carlos Guestrin. "why should i trust you?": Explaining the predictions of any classifier, 2016.
- [35] Ribana Roscher, Bastian Bohn, Marco F Duarte, and Jochen Garcke. Explainable machine learning for scientific insights and discoveries. *Ieee Access*, 8:42200–42216, 2020.
- [36] Haşim Sak, Andrew Senior, and Françoise Beaufays. Long short-term memory based recurrent neural network architectures for large vocabulary speech recognition. *arXiv preprint arXiv:1402.1128*, 2014.
- [37] Matthias Schnaubelt, Thomas G Fischer, and Christopher Krauss. Separating the signal from the noise—financial machine learning for twitter. *Journal of Economic Dynamics and Control*, 114:103895, 2020.
- [38] Sarah Schwettmann, Tamar Shaham, Joanna Materzynska, Neil Chowdhury, Shuang Li, Jacob Andreas, David Bau, and Antonio Torralba. Find: A function description benchmark for evaluating interpretability methods. *Advances in Neural Information Processing Systems*, 36, 2024.
- [39] Avanti Shrikumar, Peyton Greenside, and Anshul Kundaje. Learning important features through propagating activation differences. In *International conference on machine learning*, pages 3145–3153. PMLR, 2017.
- [40] Karen Simonyan and Andrew Zisserman. Very deep convolutional networks for large-scale image recognition. *arXiv preprint arXiv:1409.1556*, 2014.
- [41] Karen Simonyan, Andrea Vedaldi, and Andrew Zisserman. Deep inside convolutional networks: Visualising image classification models and saliency maps. *arXiv preprint arXiv:1312.6034*, 2013.

- [42] Will Cukierski Soraya Jimenez. Santander customer satisfaction, 2016. URL <https://kaggle.com/competitions/santander-customer-satisfaction>.
- [43] Mukund Sundararajan, Ankur Taly, and Qiqi Yan. Axiomatic attribution for deep networks. In *International conference on machine learning*, pages 3319–3328. PMLR, 2017.
- [44] Christian Szegedy, Wei Liu, Yangqing Jia, Pierre Sermanet, Scott Reed, Dragomir Anguelov, Dumitru Erhan, Vincent Vanhoucke, and Andrew Rabinovich. Going deeper with convolutions. In *Proceedings of the IEEE conference on computer vision and pattern recognition*, pages 1–9, 2015.
- [45] Satoshi Tsutsui, Winnie Pang, and Bihan Wen. Wbcatt: A white blood cell dataset annotated with detailed morphological attributes. *Advances in Neural Information Processing Systems*, 36, 2024.
- [46] Ashish Vaswani, Noam Shazeer, Niki Parmar, Jakob Uszkoreit, Llion Jones, Aidan N Gomez, Łukasz Kaiser, and Illia Polosukhin. Attention is all you need. *Advances in neural information processing systems*, 30, 2017.
- [47] Lijie Wang, Yaozong Shen, Shuyuan Peng, Shuai Zhang, Xinyan Xiao, Hao Liu, Hongxuan Tang, Ying Chen, Hua Wu, and Haifeng Wang. A fine-grained interpretability evaluation benchmark for neural nlp. *arXiv preprint arXiv:2205.11097*, 2022.
- [48] Pete Warden. Speech commands: A dataset for limited-vocabulary speech recognition, 2018.
- [49] Bourhan Yassin, inversion, Jack L., Mahreen Qazi, and Zephyr Gold. Rainforest connection species audio detection, 2020. URL <https://kaggle.com/competitions/rfcx-species-audio-detection>.
- [50] Matthew D Zeiler and Rob Fergus. Visualizing and understanding convolutional networks. In *Computer Vision—ECCV 2014: 13th European Conference, Zurich, Switzerland, September 6–12, 2014, Proceedings, Part I 13*, pages 818–833. Springer, 2014.
- [51] Daochen Zha, Zaid Pervaiz Bhat, Kwei-Herng Lai, Fan Yang, Zhimeng Jiang, Shaochen Zhong, and Xia Hu. Data-centric artificial intelligence: A survey, 2023.
- [52] Zhenfei Zhang and Tien D Bui. Attention-based selection strategy for weakly supervised object localization. In *2020 25th International Conference on Pattern Recognition (ICPR)*, pages 10305–10311. IEEE, 2021.
- [53] Zhenfei Zhang, Ming-Ching Chang, and Tien D Bui. Improving class activation map for weakly supervised object localization. In *ICASSP 2022-2022 IEEE International Conference on Acoustics, Speech and Signal Processing (ICASSP)*, pages 2624–2628. IEEE, 2022.
- [54] Bolei Zhou, Aditya Khosla, Agata Lapedriza, Aude Oliva, and Antonio Torralba. Learning deep features for discriminative localization, 2015.

A Appendix

A.1 Background

A.1.1 Problem Definition

When low SNR data is mentioned in this work, we specifically refer to the ratio of predictive features to irrelevant features as low and they are fed into the neural networks through independent channels. More formally, given a vectorized input $x = [x_0, \dots, x_i, \dots, x_m]$ where x_i are independent of each other, a small portion of $k \ll m$ features are predictive while all the others are irrelevant to a task to predict $y = f(x)$. A naive example can be an intrinsic single variate symbolic quadratic function.

$$y = x_0^2, x = [x_0, x_1, \dots, x_m] \quad (4)$$

As demonstrated in Figure 1d, neural networks exhibit significant resilience against noise from irrelevant feature channels, effectively focusing on the predictive features. This notable strength highlights their potential utility in feature selection tasks. In this paper, we only discuss the case of selecting features from semantically aligned

Feature selection involves reducing the number of input variables used to develop a predictive model. In traditional machine learning, several approaches to feature selection are commonly employed, including univariate filtering, embedding, and wrapper methods.

Recursive Feature Selection (RFE) is a prominent wrapper method that begins with the full set of features and progressively eliminates them. In each iteration, RFE trains a transparent statistical model and removes a certain fraction of the least important features based on the coefficients. However, this approach faces challenges when applied to neural networks due to the networks' opaque nature. Further, neural networks do not readily provide a straightforward way to rank features, rendering traditional RFE techniques inapplicable.

A.1.2 Post-hoc Local Attribution Methods

Attribution is an approach to explain a single prediction of a black-box model in a post-hoc manner. Attribution methods attribute a deep network's prediction to its input features. In other words, for a particular instance, they assign a scalar value to each feature to denote its influence on the prediction through a deep network. Attribution methods have been used to discover influential features and decipher what the neural networks have learned.

Definition 1 Suppose we have a function $F : R_m \rightarrow [0, 1]$ that represents a deep network, and an input $x = (x_1, \dots, x_m) \in R_m$. Attribution of the prediction at input x relative to a baseline input \bar{x} is a vector $A_F(x, \bar{x}) = (a_1, \dots, a_m)$, where a_i is the contribution of x_i to the prediction $F(x)$.

We study a few popular attribution methods ([2]), such as Saliency ([41]), Integrated Gradient ([43]), DeepLift ([39]), and Feature Ablation [50]). **The baseline inputs \bar{x} are always zero-tensors across all experiments in this paper.** All experiments are run on RTX 3080 with Pytorch implementations.

Saliency (SA) is the pure gradient of the function f with respect to the input features.

$$a_i = \frac{\partial F(x)}{\partial x_i} \quad (5)$$

Integrated Gradient (IG) computes the integral of gradients while the input varies along a linear path from a baseline \bar{x} to x (normally zeros). In the implementation, α is discretized into 10 steps.

$$a_i = (x_i - \bar{x}_i) \cdot \int_{\alpha=0}^1 \frac{\partial F(\tilde{x})}{\partial \tilde{x}_i} \Big|_{\tilde{x}=\bar{x}+\alpha(x-\bar{x})} d\alpha \quad (6)$$

ID	# features	Formulas
1	1	a
2	1	a^2
3	1	$\frac{2}{a^2+1} - 1$
4	1	$\sin(a)$
5	1	$\exp(a) - 1.5$
6	1	$2 \log(a^2 + 1) - 1$
7	2	$0.25a^3 + 0.75b^2$
8	3	$0.5a^3 + 0.75b^2 + a \cdot c$
9	4	$0.5 \exp(a) \cdot \sin(b) - 0.25 \frac{\cos(d)^5}{c^2+1}$
10	5	$0.5(a-b)^2 + 0.2(c+d \cdot e)^3 - 0.5$
11	6	$0.5 \cos(a) \cdot \tan(b) - \frac{\log((c-d)^2+1)}{(e+f+1)^2+1}$
12	7	$0.5 \frac{(b-c)^2}{a^2+1} + \tan(d) \cdot \log(e^2+1) + 0.5 \cos(f) \cdot \sin(g)$
13	8	$a + \frac{1}{2}b^2 + \frac{1}{3}c^3 + \frac{1}{4}d^4 + \frac{1}{5}e^5 + \frac{1}{6}f^6 + \frac{1}{7}g^7 + \frac{1}{8}h^8$
14	9	$0.5 \frac{a-1}{b^2+1} - 0.5 \frac{c^3}{d^2+1} + 0.5 \frac{e^5}{f^2+1} - 0.5 \frac{g^7}{h^2+1} + 0.5 \tan(i) + 0.5$
15	10	$0.5 \sin(a) - 0.5b^3 - \log(c^2+1) + 0.5((d+e)^2+1)^{\frac{1}{2}} - 0.5 * \cos(f) \cdot g + h \cdot \frac{i^2}{(1-j)^2+1} - 0.5$

Table 5: The formulas of symbolic functions and the number of predictive features in each function.

DeepLift (DL) decomposes the output prediction of f by backpropagating the contributions of all neurons in the network to every feature of the input with the rescale rule. In practice, it provides attribution quality comparable with IG but faster.

$$r_i^{(l)} = \sum_j \frac{z_{ji} - \bar{z}_{ji}}{\sum_{i'} z_{ji} - \sum_{i'} \bar{z}_{ji}} r_j^{l+1}, \quad z_{ji} = w_{ji}^{(l+1,l)} \bar{x}_i^{(l)} \quad (7)$$

$$a_i = r_i^{(0)}, \quad r^{(L)} = F(x) - F(\bar{x}) \quad (8)$$

Feature Ablation (FA) is a perturbation-based approach to computing attribution which computes the difference in $f(x)$ by replacing each feature x_i with a baseline \bar{x}_i (normally zero).

$$a_i = F(x) - F(x_{[x_i=\bar{x}_i]}) \quad (9)$$

A.2 Symbolic Function Regression Task

A.2.1 Data Details

We created 15 formulas using different symbolic functions. The symbolic functions are shown in the Table 5. One benefit of using symbolic functions to create data is that the true values of these functions, derivatives, and integrals are strictly obtainable via the "SymPy" Python library. Each x_i feature is randomly sampled from a normal distribution with a mean of 0 and variance of 0.33, then being clipped into the range of [-1, 1].

Let $x' = [x_0, \dots, x_m]$ denote the vector predictive features and f as the human-defined intrinsic function. The numbers of predictive features range from 1 to 10 and the functions are combinations of primitive math (e.g. polynomial, trigonometric, and exponential) functions. We create a regression task by evaluating $y = f(x')$, where f is the intrinsic symbolic function without any feature or label noise involved. The black-box model $F(x) = F(x_i, \dots, x_m)$ is obtained by training via noisy features and labels. We originally evaluate the $UScore$ of feature attribution methods with ground truth values. We compute the ground truth values of FA (10), SA (11), and IG (12) using

$$\Delta f_i(x; \bar{x}) = f(x) - f(x_{[x_i=\bar{x}_i]}) \quad (10)$$

$$\nabla f_i = \frac{\partial y}{\partial x_i} \quad (11)$$

$$\blacktriangle f_i(\bar{x}) = \sum_{s=1}^S \Delta f_i(\bar{x} + \frac{s}{S}(x - \bar{x}); \bar{x} + \frac{s-1}{S}(x - \bar{x})) \quad (12)$$

where $\bar{x} = [\bar{x}_0, \dots, \bar{x}_m]$ denotes the vector of baseline input to compute the contribution of x_i relative to \bar{x}_i to the target $f(x)$.

A.2.2 Supplementary Experiment Results

We plot the $UScores$ in 8, which differs from the results in the main context identifying important features. The default training configurations are the same as the main context. From the plots, we see similar trends of change as the main context. However, in the precision to estimate ground truth values, IG is better than FA and then SA. Although SA is not accurately approximating the derivatives, it is better at identifying the most predictive features.

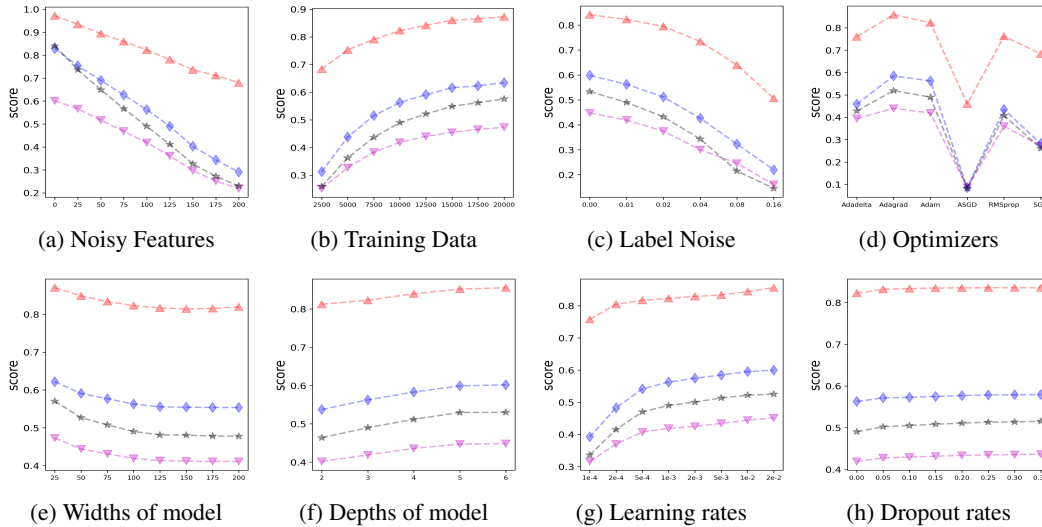


Figure 8: Experimental results on symbolic functional data using MLP regressors differentiated by varying factors. For each subplot, we only change one factor from the default configuration. \blacktriangle , \blacktriangledown , \blacklozenge , and \blackstar denote the $UScore$ of prediction, SA, IG, and FA methods w.r.t. the ground truth values respectively.

A.3 Vision Task

A.3.1 Dataset Details

Our synthetic image data consists of a background image and a foreground image. The foreground image represents the predictive features and the label is the target to predict while the background image represents features irrelevant to the classification task. We use CIFAR10, an image dataset with 10 classes of common objects, as the foreground dataset. The 10 classes are *airplanes, cars, birds, cats, deer, dogs, frogs, horses, ships, trucks*. We use Flowers102, an image classification dataset consisting of 102 flower categories, as the structural background dataset. The background image size is 224. The foreground image size is 32. There are 3 channels. These two datasets are loaded through the Pytorch default interfaces. The train split is created from the train splits of both datasets. The validation split is created from the validation split of Flower102 and the non-training split of CIFAR10. Thus, it's guaranteed that there's no data leakage. Each image is created by combining a foreground image with a sampled background image in its split with random positions (if needed). There are 50000 images in the train split and 10000 images in the validation split. There are four sub-directories in the dataset: RBF, RBR, SB, and SBR. We provide a "meta_data.csv" file in each sub-directory containing the image id, foreground label, x-axis position, and y-axis position. We study the noise conditions to get insights into the positional issue, registration issue, and structural encoding issue.

A.3.2 Experiment Details

The models are trained for 30 epochs and the batch size is 128. The number of iterations for the first restart is 30. We show the examples of the retrieved region (red rectangle) and the true region (yellow rectangle) of attribution methods in Figure 9. In the experiments, we smoothen the saliency maps

by a 2D Gaussian filter with $\sigma = 6$. The pre-trained vision models are loaded from default Pytorch implementations trained for 30 epochs. For easy feature ablation, we defined a mask with 49 square patches of size 32×32 .

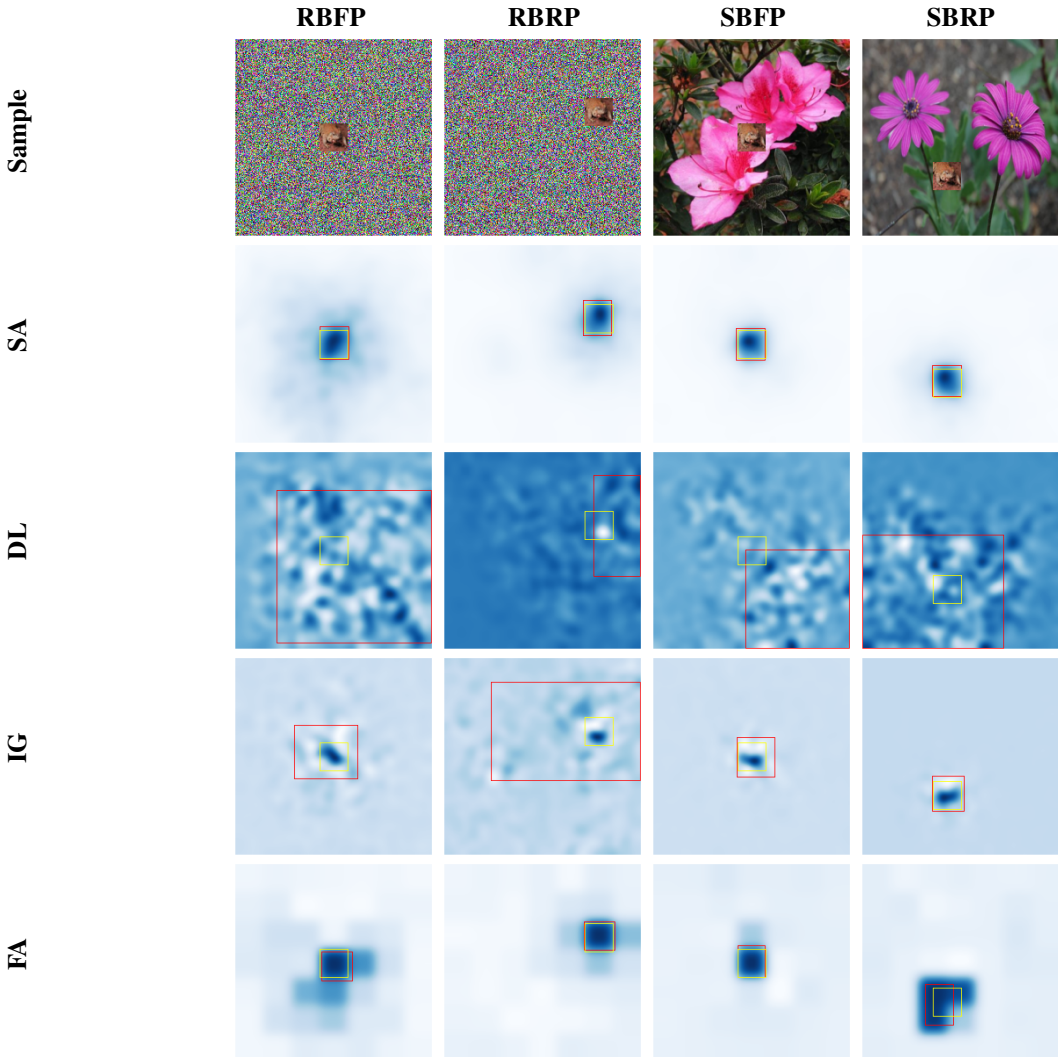


Figure 9: The examples of vision data and saliency maps of attribution methods. The foreground images can be placed at a fixed position (center) across instances or randomly. The background images can be generated by Gaussian noise or images of flowers. The red boxes denote the estimated positions of predictive features of attribution methods and the yellow boxes denote the true positions.

A.4 Audio Task

A.4.1 Dataset Details

Similarly, our synthetic audio data is composed of foreground sounds and background sounds. Here we use Speech Commands to support the foreground sounds classification task, which is a dataset of 35 commands spoken by different people. The 35 classes are *backward, bed, bird, cat, dog, down, eight, five, follow, forward, four, go, happy, house, learn, left, marvin, nine, no, off, on, one, right, seven, sheila, six, stop, three, tree, two, up, visual, wow, yes, zero*. As for the structural background sound, we use animals' sounds of Rainforest Connection Species data from Kaggle. In the dataset, all audio recordings are regularized into 1 second long by clipping and resampling. The sampling rate is uniformly 16000 per second. The foreground sound as well as the background sound are stacked in the "channel" dimension. Each channel represents a single sound. In our

experiment, each audio data possesses 10 channels with 1 channel as the foreground sound and 9 channels as the background sound. The visualizations of 1D waveform and spectrogram audio data are shown in Figure 10. All channels are normalized to the range of $[-1, 1]$. In order to benchmark regular architectures specifically designed for sequential data, we use waveform of audio data in all experiments. We created 4 subsets RBFP, RBRP, SBFP, and SBRP, like the vision dataset, where the position refers to the channel of speech command sound and the structure refers to the semantic meaning of background sound. Since all models failed to converge for RBRP and SBRP. We dropped the results for them. The dataset consists of 84843 training waves and 9981 validation waves for each noise condition. We provide a “meta_data.csv” file containing the audio id, audio label, and predictive channel position. As for data with structural background, the train set is generated by training data of Speech Commands and training data of Rain Forest Species while the validation set is generated from the validation data of Speech Commands and testing data of Rain Forest Species. Thus, it’s guaranteed that there’s no data leakage.

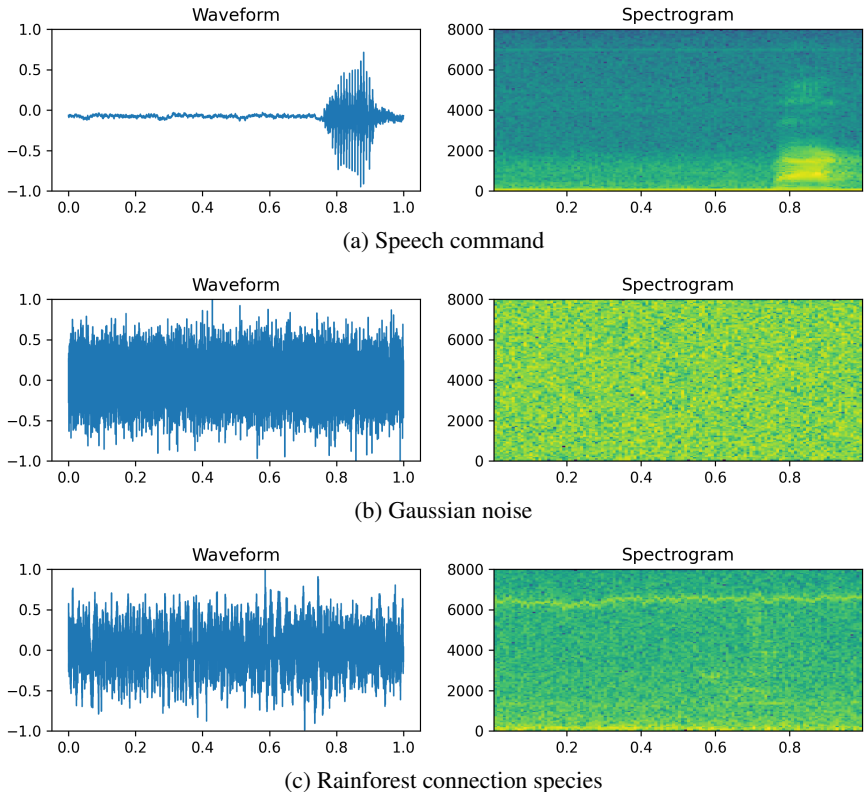


Figure 10: The examples of sources to construct synthetic audio data. Figure (a) is the foreground predictive feature while (b) and (c) are background features that are irrelevant to the classification task.

A.4.2 Experiment Details

In the experiments on audio tasks, we train the models for 30 epochs and the batch size is 128. The number of iterations for the first restart is 30. The audio models are implemented using Pytorch. The hidden dimensions are 60 and the number of hidden layers is 3 for all models. The inputs are first passed into a 1D convolutional layer to learn some inductive bias and the output linear layers are fed with the max 1D-pooling intermediate outputs on the time sequence axis.

A.5 RFEwNA Classification Task

A.5.1 Dataset Details

The Santander Customer Satisfaction dataset from Kaggle is a popular dataset used in a competition aimed at helping Santander Bank to identify dissatisfied customers at an early stage. The ability to predict customer satisfaction based on historical data allows Santander to take proactive steps to improve a customer’s happiness before it’s too late, thereby enhancing customer loyalty and retention.

The dataset is typically provided for a binary classification problem where the goal is to predict customer satisfaction based on a number of anonymized features. There are 369 anonymous features in the datasets. The original 0-1 class balance ratio is around 96% : 4%. All columns are normalized with a “*MinMaxScaler*”. We use random undersampling of the major class until the 0-1 class ratio is balanced. Finally, a total number of 6,016 samples are shuffled and split with a 4:1 ratio into training and test sets.

A.5.2 Experiment Details

The batch size is 1000, and models are trained for 500 epochs. We conducted 5 replicas of training and testing. The model is the same as the default one in the symbolic functional regression task. We use the scikit-learn implementation linear, SVM, and decision tree models and RFE. The linear model is “*sklearn.linear_model.LogisticRegression(penalty=None)*”. The SVM model is “*sklearn.svm.SVC(kernel = 'linear', probability = True)*”. The decision tree model is “*sklearn.tree.DecisionTreeClassifier()*”. Given an external estimator that assigns weights to features (e.g., the `coef_` or `feature_importances_`), RFE selects features by recursively considering smaller and smaller sets of features. 50% least important features of the currently selected set for each iteration, which is consistent with RFEwNA (our approach).

A.6 Reproducibility Checklist

All of our codes & data are accessible through <https://github.com/geshijoker/ChaosMining>. Any updates regarding data cards or metadata due to maintenance will be shown on the same project page to avoid inaccurate descriptions. If any links below are disabled or the resources are not found in the attached supplementary materials, please refer to the project page.

A.6.1 Dataset

1. The dataset is stored and maintained by *huggingface* with a “doi:10.57967/hf/2482”. The dataset card, croissant metadata (built on schema.org), and dataset viewer are automatically provided. The data is permanently available.
2. We adopt a CC BY-NC 4.0 license. We state that we bear all responsibility in case of violation of rights, etc.
3. All data use an open and widely used data format, e.g. symbolic functional data in .csv type, vision data in .png time; audio data in .wav type, and metadata with annotations in .csv type. As for the detailed way to load the data, please refer to the project page.
4. We use the huggingface community for discussion, maintenance, and troubleshooting. Additional data for other types of noise conditions or modalities will be additive to the same doi with version control. we promise to clean the data if any violation of ethics is reported.

A.6.2 Benchmark

We provide a reproducibility checklist following [31] suggested by Submission Introductions <https://neurips.cc/Conferences/2024/CallForDatasetsBenchmarks>.

1. For all **models** and **algorithms** presented, check if you include:
 - (a) A clear description of the mathematical setting, algorithm, and/or model? [Yes]
 - (b) An analysis of the complexity (time, space, sample size) of any algorithm [N/A]
 - (c) A link to a downloadable source code, with a specification of all dependencies, including external libraries. [Yes]
2. For any **theoretical claim**, check if you include
 - (a) A statement of the results. [N/A]
 - (b) A clear explanation of any assumption? [N/A]
 - (c) A complete proof of the claim. [N/A]

Since we do not have any **theoretical claim**, this part does not apply.

3. For all **figures** and **tables** that present empirical results, check if you include:

- (a) A complete description of the data collection process, including sample size. [Yes]
- (b) A link to a downloadable version of the dataset or simulation environment. [Yes]
- (c) An explanation of any data that were excluded, description of any pre-processing step. [N/A]
- (d) An explanation of how samples were allocated for training/validation/testing. [Yes]
- (e) The range of hyper-parameters considered, method to select the best hyper-parameter configuration, and specification of all hyper-parameters used to generate results. [Yes]
- (f) The exact number of evaluation runs. [Yes]
- (g) A clear definition of the specific measure or statistics used to report results. [Yes]
- (h) Clearly defined error bars. [Yes]
- (i) A description of results with a central tendency (e.g. mean) & variation (e.g. stddev). [Yes]
- (j) A description of the computing infrastructure used. [Yes]